Grid Synchronization With Selective Harmonic Detection Based on Generalized Delayed Signal Superposition

Yong Lu, Guochun Xiao, *Member, IEEE*, Xiongfei Wang, *Member, IEEE*, and Frede Blaabjerg, *Fellow, IEEE*

***Abstract*—Grid synchronization has always been an important challenge for grid-connected converters under extremely distorted grid conditions. Moreover, how to quickly and accurately extract multiple required harmonics is also essential for control systems. In this paper, two types of generalized delayed signal superposition (GDSS) operators capable of extracting any arbitrary harmonic component out of an input signal are derived. In order to show the benefits of GDSS operators, a new grid information estimation concept based on multiple GDSS operators (referred to as MGDSS-PLL) is proposed to track the fundamental and multiple targeted harmonics under single-phase and three-phase adverse grid conditions. MGDSS-PLL can be flexibly tuned to extract any harmonic components according to specific requirements within one fundamental period, and it also exhibits great robustness to grid disturbances. Simulations and experimental results are presented for verifying the performance of the MGDSS-PLL.**

***Index Terms*—Delayed signal superposition, grid synchronization, phase-locked loop, selective harmonic detection.**

I. Introduction

In RECENT years, distributed generation systems (DGSs) based on renewable energy sources (RESs) have experienced a rapid and continuous development due to the increasing demand for cleaner energy and also a flexible electric power system like the smart grid [1]–[4]. However, a high penetration level of RESs in turn challenges reliable, efficient, and safe operation of the utility grid and therefore the related grid codes become more and more rigorous [5]–[7]. Consequently, power-electronic converters, acting as energy conversion interface between the DGSs and electricity network, are required to provide stable performance and fault-ride-through capability in order to handle undesired grid perturbations (including voltage sags, system unbalance, and severe distortions) [8]–[10]. In this scenario, one of the key issues in the design of reliable controllers for these converters is the grid synchronization at the point of common coupling. Therefore, the synchronization algorithm should be accurate and robust under a variety of grid conditions and play a critical role in the control of converters [11]–[16], which is also demonstrated in Fig. 1.

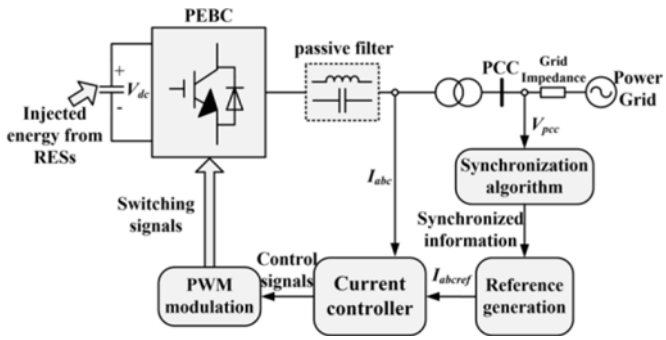

Fig. 1. General control system for power-electronic converters connected to the grid.

Synchronous reference frame phase-locked loop (SRF-PLL) is generally considered to be the most widely applied synchronization technique in both single-phase and three-phase systems considering its simple structure and satisfactory performance. However, its tracking accuracy tends to be unacceptable when the grid is polluted and/or unbalanced [17]–[19]. To improve the behavior of SRF-PLL under abnormal grid conditions, various advanced approaches have been discussed in recent years [20]–[32]. A majority of these approaches are based on adding filtering stages, which can be further categorized into two types as extended-loop-filter-based techniques and prefilter-based techniques [24]. In practical implementation, the extended-loop-filter-based methods are often preferred when only the fundamental component of the grid is required, whereas the prefilter-based synchronization techniques are generally adopted to extract the fundamental and selected harmonic components. Therefore, the prefilter-based techniques are normally considered to be more convenient for a flexible control strategy design under adverse grid conditions [25].

There are a variety types of prefilter-based synchronization techniques proposed, including decoupled synchronous

Manuscript received March 1, 2017; revised May 23, 2017; accepted June 22, 2017. Date of publication June 29, 2017; date of current version February 1, 2018. This work was supported by the National Natural Science Foundation of China under Project 51277146. Recommended for publication by Associate Editor F. W. Fuchs. *(Corresponding author: Yong Lu.)*

Y. Lu is with the School of Electronics and Control Engineering, Chang'an University, Xi'an 710064, China, and also with the State Key Laboratory of Electrical Insulation and Power Equipment, School of Electrical Engineering, Xi'an Jiaotong University, Xi'an 710079, China (e-mail: luyong@chd.edu.cn).

G. Xiao is with the State Key Laboratory of Electrical Insulation and Power Equipment, School of Electrical Engineering Xi'an Jiaotong University, Xi'an 710049, China (e-mail: xgc@mail.xjtu.edu.cn).

X. Wang and F. Blaabjerg are with the Department of Energy Technology, Aalborg University, Aalborg 9220, Denmark (e-mail: xwa@et.aau.dk; fbl@et.aau.dk).

Color versions of one or more of the figures in this paper are available online at http://ieeexplore.ieee.org.

Digital Object Identifier 10.1109/TPEL.2017.2721461

reference-frame PLL [20], [26], sinusoidal signal integrator PLL [27], signal reforming PLL [28], moving average filter PLL [29], [30], double second-order generalized integrator PLL (DSOGI-PLL) [31], [32], and delayed signal cancelation PLL [33], [34], but these PLLs rarely give satisfactory harmonic detection performance when considering their overall evaluation in terms of the response time, steady-state error, and robustness. Then, in [35]–[37], solutions based on harmonic decoupling network (HDN) are proposed with improved harmonic detection performance. These techniques can operate fast and accurately under highly distorted grid and also allow the estimation of multiple harmonic components. However, these schemes are generally sensitive to unconsidered harmonics, and their dynamic responses are still not satisfactory (from one to several fundamental cycles), especially under grid disturbances. For instance, the synchronization method introduced in [35], denoted as multiple second-order generalized integrator frequency-locked loop (MSOGI-FLL), consists of multiple DSOGIs tuned at different harmonics of the fundamental grid frequency and an HDN that decouples the interactions of different harmonic components on the input signal of these DSOGIs. Thus, the MSOGI-FLL can detect both the fundamental and the harmonic sequences even under highly polluted grid conditions. However, since there exists a tradeoff between the selectivity and settling time of the SOGI operator, the number of DSOGI subsystems should be equal to the number of significant harmonics contained in the distorted grid in order to ensure an acceptable dynamic response. Hence, any unconsidered harmonics will affect the steady-state error of the HDN and the calculated results.

In this paper, two types of generalized delayed signal superposition (GDSS) operators are derived based on the delayed signal superposition operators presented in [38], and they can extract any selected harmonic component out of the input signal with the response time as short as half a fundamental period. The obtained GDSS operators can be flexibly configured to improve the performances of grid synchronization and harmonic detection algorithms according to different grid conditions or control requirements. Then, a novel grid synchronization technique capable of detecting fundamental and multiple targeted harmonics is introduced for both single-phase and three-phase systems under extremely distorted grid conditions. The proposed system is denoted as multiple GDSS phase-locked loop (MGDSS-PLL) since it contains multiple GDSS operators tuned at the different harmonics, which cooperatively work as a set of selective filters. Compared to the MSOGI technique, the GDSS operators are more selective such that the design of each GDSS submodule is independent, and there are no interactions between the different harmonic orders. Hence, the number of GDSS operators only depends on the number of interested harmonics, and these operators are insensitive to unconsidered harmonic components. Moreover, the presented MGDSS-PLL is robust to small variations of the fundamental frequency and exhibits great robustness against different grid perturbations. It should be mentioned that the GDSS is similar to the cascaded delayed signal cancellation (CDSC) introduced in [39] as they both originate from the concept of signal delay. However, differing from the CDSC, the proposed GDSS is derived through an algebraic recursive procedure, which provides an easier parameter design process and also a more intuitive harmonic elimination principle. Additionally, no magnitude or phase angle correction block is needed for the MGDSS-PLL method. In the paper, simulations and experimental results are presented to verify the performance of the proposed GDSS operators as well as the MGDSS-PLL technique.

II. GDSS Operators

Any voltage/current signal $u(t)$ can be regarded as a combination of the fundamental and harmonics. Then, $u(t)$ is described as follows:

$$u(t) = \sum_{h=1}^{H} U_h \cos(h\omega t + \varphi_h) \tag{1}$$

where h is the harmonic order (for fundamental component, $h = 1$), H represents the maximum harmonic order considered, ω and φ_h are the fundamental frequency and initial phase of the h-order harmonics, respectively. Two different types of generalized delayed signal operators (GDS1 and GDS2) for $u(t)$ are considered in this paper:

$$\mathrm{GDS1}[u(t)] = u\left(t - \frac{k}{h_s n}T\right)\cos\frac{2k\pi}{n} \tag{2}$$

$$\mathrm{GDS2}[u(t)] = u\left(t - \frac{k}{h_s n}T\right)\sin\frac{2k\pi}{n} \tag{3}$$

where T is the fundamental period, h_s is the harmonic order to be detected, and n, k are arbitrary integers. If GDS1[$u(t)$] and GDS2[$u(t)$] are added with k ranging from 0 to $m\,(m < h_s n)$ and then multiplied by $2/(m+1)$, two types of GDSS operators can be constructed as follows:

$$\mathrm{GDSS1}[u(t)] = \frac{2}{m+1}\sum_{k=0}^{m} u\left(t - \frac{k}{h_s n}T\right)\cos\left(\frac{2k\pi}{n}\right) \tag{4}$$

$$\mathrm{GDSS2}[u(t)] = \frac{2}{m+1}\sum_{k=0}^{m} u\left(t - \frac{k}{h_s n}T\right)\sin\left(\frac{2k\pi}{n}\right) \tag{5}$$

When the h-order harmonic $u_h(t) = U_h\cos(h\omega t + \varphi_h)$ is considered, (4) can be further derived as follows:

$$\mathrm{GDSS1}[u_h(t)] = \frac{2}{m+1}\sum_{k=0}^{m} U_h\cos\left(\alpha - \frac{2hk\pi}{h_s n}\right)\cos\left(\frac{2k\pi}{n}\right) \tag{6}$$

where α represents the phase angle of $u_h(t)$ and $\alpha = h\omega t + \varphi_h$. Then, (6) can be rearranged to be

$$\mathrm{GDSS1}[u_h(t)] = \frac{U_h}{m+1}\sum_{k=0}^{m}[\cos(\alpha - 2kA) + \cos(\alpha - 2kB)] \tag{7}$$

$$A = \frac{(h - h_s)}{h_s n}\pi \tag{8}$$

$$B = \frac{(h + h_s)}{h_s n}\pi. \tag{9}$$

Fig. 2. Illustration of GDSS-based QSG method.

TABLE I
RELATIONSHIPS AMONG h_s, m, n, h_i

h_s	m	n	h_i
1	14	15	1, 14, 16, 29, 31 . . .
3	14	5	3, 12, 18, 27, 33 . . .
4	15	4	4, 12, 20, 28, 36 . . .
5	14	3	5, 10, 20, 25, 35 . . .
7	20	3	7, 14, 28 . . .
8	23	3	8, 16, 32 . . .
9	26	3	9, 18, 36 . . .

According to the certain sums of trigonometric functions provided in [40], (7) can be further simplified as follows:

$$\mathrm{GDSS1}[u_h(t)] = \begin{cases} G(\mathrm{CD}\csc A + \mathrm{EF}\csc B) & h \neq h_i \\ U_h\cos\alpha + \mathrm{GEF}\csc B & h = h_s(jn+1) \\ U_h\cos\alpha + \mathrm{GCD}\csc A & h = h_s(jn-1) \end{cases} \tag{10}$$

where $C = \cos(\alpha - mA)$, $D = \sin[(m+1)A]$, $E = \cos(\alpha - mB)$, $F = \sin[(m+1)B]$, $h_i = h_s(jn \pm 1)$, and j is a natural number. The same derivation process can be applied to analyze (5) and a similar expression can be obtained as follows:

$$\mathrm{GDSS2}\,[u_h(t)] = \begin{cases} G(\mathrm{JD}\csc A + \mathrm{KF}\csc B) & h \neq h_i \\ U_h\sin\alpha + \mathrm{GKF}\csc B & h = h_s(jn+1) \\ U_h\sin\alpha + \mathrm{GJD}\csc A & h = h_s(jn-1) \end{cases} \tag{11}$$

where $J = \sin(\alpha - mA)$ and $K = \sin(\alpha - mB)$.

As can be solved from (10), if D and F are set to zero with $m = h_s n - 1$, *GDSS1* operator will exhibit a zero gain for any harmonic components at $h \neq h_i$, but a unity gain and zero phase shift for the harmonic components at $h = h_i$, including the selected harmonic order h_s. The same conclusion can be drawn for the *GDSS2* except that it will introduce an extra $-\pi/2$ phase shift to the harmonics at $h = h_i$. Therefore, *GDSS1* and *GDSS2* can be configured as a quadrature signal generation (QSG) method, and it can generate two pure quadrature signals at any targeted harmonic order h_s with properly designed m and n. Fig. 2 illustrates the QSG algorithm based on the GDSS operators (GDSS-QSG), where V_{hs} represents the h_s-order harmonic component targeted at the input signal V_{in} and $q = e^{-j\pi/2}$ denotes a $\pi/2$ phase delay operator. Typical parameter designs of m, n, h_s, and h_i can be calculated and they are given in Table I.

As can be seen from (4) and (5), the maximum delay time for *GDSS1* and *GDSS2* is $mT/h_s n$, which enables a fast harmonic detection with the response time less than one fundamental period. Additionally, with the further observation on (10) and (11), for the applications where the even-order harmonics are considered to be noncritical components (like in single-phase systems), m can be redesigned to $h_s n/2 - 1$ ($h_s \times n$ is an even number) and the overall time delay will be significantly reduced to less than half a fundamental cycle. In this situation, the harmonic selection performance of *GDSS1* and *GDSS2* remains nearly the same, except that the even-order harmonics will not be completely eliminated.

In a practical implementation, GDSS-QSG will be realized with digital signal processor and thus discretization is needed for (4) and (5). If the sampling points of $u(t)$ is set to N_S within a fundamental cycle, the discretized expression of the GDSS-QSG operator can be written as follows:

$$\begin{bmatrix} V_{hs}[i] \\ qV_{hs}[i] \end{bmatrix} = \begin{bmatrix} \frac{2}{m+1}\sum_{k=0}^{m} u\left[i - \frac{k}{h_s n}N_S\right]\cos\left(\frac{2k\pi}{n}\right) \\ \frac{2}{m+1}\sum_{k=0}^{m} u\left[i - \frac{k}{h_s n}N_S\right]\sin\left(\frac{2k\pi}{n}\right) \end{bmatrix} \tag{12}$$

According to (12), the *GDSS1* and *GDSS2* can be regarded as two finite impulse responses filters, and its performance is similar to the comb filter developed in the digital signal processing theory [41]. In Fig. 3, the frequency responses of the GDSS-QSG at $h_s = 4$ and 7 are demonstrated, based on the parameters provided in Table I, in order to verify the previous analysis. Fig. 4 presents the frequency responses of the fast GDSS-QSG at $h_s = 5$ and 7 when the even-order harmonics are not considered. In Fig. 4(a) and (b), $m = 14$, $n = 6$; in Fig. 4(c) and (d), $m = 20$, $n = 6$. As can be seen from Figs. 3 and 4, the GDSS operators are rather selective and can be flexibly configured for the different applications. As also indicated by the presented frequency responses, gains decrease abruptly at frequencies deviated from the selected harmonics; thus, the interharmonics/subharmonics can be suppressed by the GDSS operators, although not completely eliminated.

III. MGDSS-PLL FOR SINGLE-PHASE AND THREE-PHASE APPLICATIONS

As previously mentioned, the proposed GDSS operators can be flexibly configured with different parameters to eliminate the unwanted harmonics in the input signal and extract only the desired harmonic component. According to the theoretical analysis, the GDSS operators have very short transient and are quite selective. Therefore, they can be readily adopted to enhance the performance of grid synchronization or harmonic detection algorithms under adverse grid conditions since the grid information sensed is highly distorted. In this section, presented as two possible solutions, multiple GDSS operators tuned at the different frequencies are utilized collaboratively in both single-phase and three-phase systems to obtain the grid fundamental and multiple harmonic components. The new detection configurations in these two applications are both denoted as MGDSS-PLL.

A. MGDSS-PLL for Single-Phase Applications

The main structure of the MGDSS-PLL for single-phase applications is demonstrated in Fig. 5, where V_{in} is the single-phase input signal, θ and V_1 denote for the computed

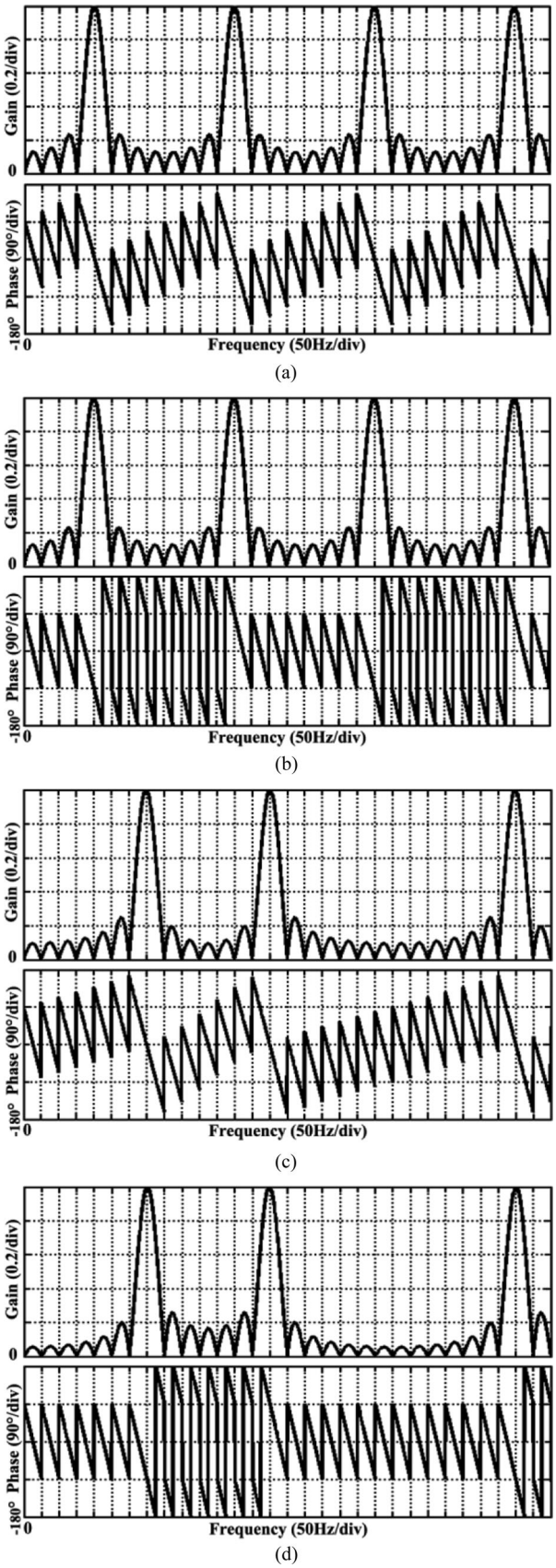

Fig. 3. Frequency responses of GDSS-QSG at $h_s = 4 \text{ and } 7$. (a) Frequency response of *GDSS*1 at $h_s = 4$. (b) Frequency response of *GDSS*2 at $h_s = 4$. (c) Frequency response of *GDSS*1 at $h_s = 7$. (d) Frequency response of *GDSS*2 at $h_s = 7$.

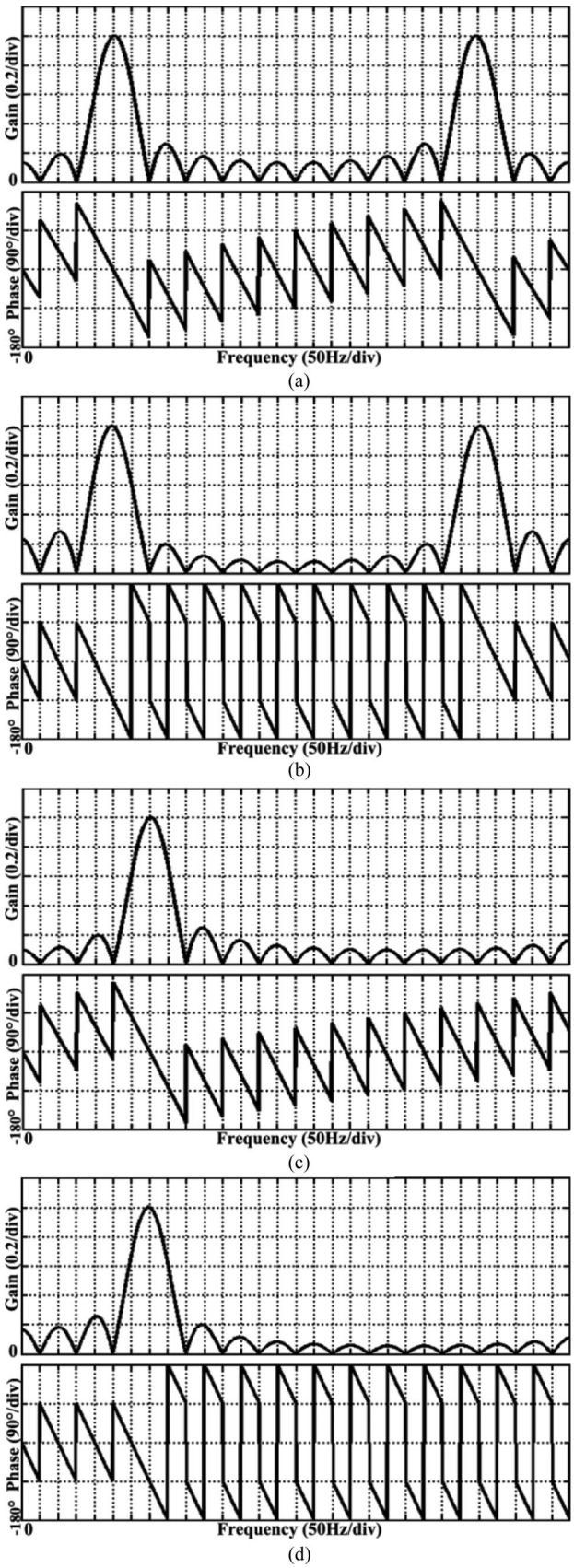

Fig. 4. Frequency responses of fast GDSS-QSG at $h_s = 5 \text{ and } 7$. (a) Frequency response of fast *GDSS*1 at $h_s = 5$. (b) Frequency response of fast *GDSS*2 at $h_s = 5$. (c) Frequency response of fast *GDSS*1 at $h_s = 7$. (d) Frequency response of fast *GDSS*2 at $h_s = 7$.

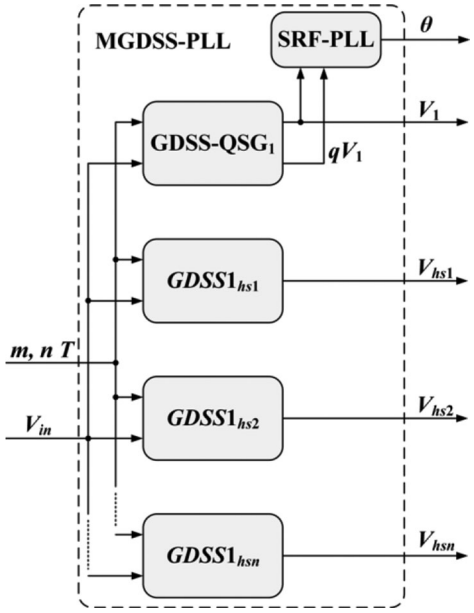

Fig. 5. Configuration of the single-phase MGDSS-PLL.

fundamental phase and voltage, respectively, $hs1$, $hs2 \ldots$ hsn are multiple harmonic orders targeted, V_{hs1}, $V_{hs2} \ldots V_{hsn}$ represent the extracted harmonic components at corresponding frequencies, $GDSS1_{hs1}$, $GDSS1_{hs2} \ldots GDSS1_{hsn}$ stand for the *GDSS*1 operators tuned at these harmonic orders. As can be seen from Fig. 5, MGDSS-PLL consists of multiple GDSS operators tuned at different frequencies and working in parallel as a set of selective filters. A standard SRF-PLL structure is adopted here to estimate the phase of the fundamental component. According to the structure diagram demonstrated, the operation principle of the MGDSS-PLL and the function of each submodular can be concluded and described as follows.

1) Single-phase input signal V_{in} is sampled and the contained harmonic components will be eliminated by the GDSS-QSG submodular tuned at the fundamental frequency. Therefore, two pure quadrature signals will be generated through this process and then fed to the SRF-PLL block.
2) A standard SRF-PLL structure introduced in [31] is applied here to track the fundamental phase θ. Since the input of SRF-PLL is clean, the control bandwidth of the SRF-PLL can be designed to be high in order to ensure a good dynamic. How to design the PI parameters is described in [31] and will not be included in this paper.
3) Meanwhile, the harmonics of interest are extracted by multiple *GDSS1* operators working in parallel and the irrelevant frequency components will be completely filtered. Since these GDSS operators are rather selective, there will be no interaction between different harmonics. Consequently, the design of each *GDSS1* operator is independent and only focused on the particular harmonics.
4) Finally, the obtained grid information, including the fundamental phase, fundamental component and multiple harmonics, is fed to the control system for reference generation or related computation.

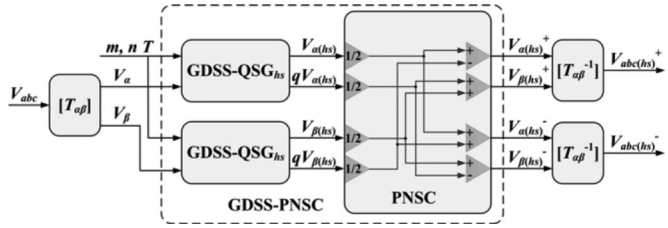

Fig. 6. Structure diagram of the GDSS-PNSC.

B. MGDSS-PLL for Three-Phase Applications

With an extra concern for the sequence components detection, the MGDSS-PLL structure proposed for single-phase applications can be readily implemented in three-phase applications under an $\alpha\beta$ reference frame. Therefore, before the three-phase MGDSS-PLL configuration is presented, a harmonic sequence component extraction algorithm based on a positive- and negative-sequence calculator (PNSC) and GDSS operators is derived in the first place.

The derivation process of the PNSC is introduced in [35], and the obtained expressions can be directly adopted in this paper. According to [35], the positive- and negative-sequence components in the $\alpha\beta$ reference frame can be calculated as follows:

$$\begin{bmatrix} V_\alpha^+ \\ V_\beta^+ \end{bmatrix} = [T_{\alpha\beta+}] \begin{bmatrix} V_\alpha \\ V_\beta \end{bmatrix}; \quad [T_{\alpha\beta+}] = \frac{1}{2} \begin{bmatrix} 1 & -q \\ q & 1 \end{bmatrix} \tag{13}$$

$$\begin{bmatrix} V_\alpha^- \\ V_\beta^- \end{bmatrix} = [T_{\alpha\beta-}] \begin{bmatrix} V_\alpha \\ V_\beta \end{bmatrix}; \quad [T_{\alpha\beta-}] = \frac{1}{2} \begin{bmatrix} 1 & q \\ -q & 1 \end{bmatrix} \tag{14}$$

where V_α, V_β are the signals transformed from the *abc* stationary frame by using the *Clark* transformation, and V_α^+, V_β^+, V_α^-, V_β^- represent the positive- and negative-components in the $\alpha\beta$ reference frame. The expression of the *Clarke* transformation $T_{\alpha\beta}$ is written as follows:

$$[T_{\alpha\beta}] = \sqrt{\frac{2}{3}} \begin{bmatrix} 1 & -\frac{1}{2} & -\frac{1}{2} \\ 0 & \frac{\sqrt{3}}{2} & -\frac{\sqrt{3}}{2} \end{bmatrix} \tag{15}$$

As can be seen from (13) and (14), the quadrature signals of V_α, V_β are required for the calculation of the desired V_α^+, V_β^+, V_α^-, V_β^-. Therefore, the aforementioned GDSS-QSG can be applied to provide these quadrature signals and the unwanted harmonic components will also be eliminated through this process. Fig. 6 illustrates the structure diagram of the discussed harmonic sequence components extraction algorithm, which is marked as GDSS-PNSC.

In Fig. 6, V_{abc} represents the three-phase voltage/current signal to be estimated; $V_{\alpha(hs)}$, $V_{\beta(hs)}$ are the targeted h_s-order harmonic under the $\alpha\beta$ reference frame; $V_{\alpha(hs)}^+$, $V_{\beta(hs)}^+$, $V_{\alpha(hs)}^-$, $V_{\beta(hs)}^-$ denote the extracted positive and negative sequence

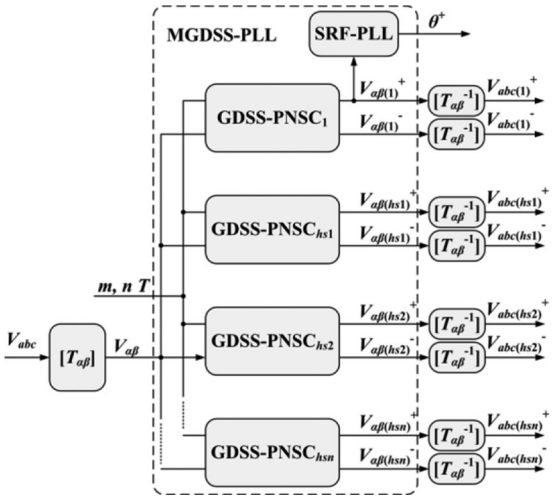

Fig. 7. Configuration of the three-phase MGDSS-PLL.

components of $V_{\alpha(hs)}$ and $V_{\beta(hs)}$; $V^+_{abc(hs)}$ and $V_{abc(hs)}{}^-$ are, respectively, the computed positive and negative components of V_{abc}; $\mathrm{GDSS}-\mathrm{QSG}_{hs}$ stands for the GDSS-QSG operator tuned at the h_s-order harmonic. Moreover, $T^{-1}_{\alpha\beta}$ is the inverse *Clark* transformation and it is given as follows:

$$\left[T^{-1}_{\alpha\beta}\right] = \sqrt{\frac{2}{3}} \begin{bmatrix} 1 & 0 \\ -\frac{1}{2} & \frac{\sqrt{3}}{2} \\ -\frac{1}{2} & -\frac{\sqrt{3}}{2} \end{bmatrix} \tag{16}$$

Then, if the GDSS operators in Fig. 5 are substituted with GDSS-PNSC blocks and the required transformation are added, three-phase MGDSS-PLL capable of detecting fundamental information and multiple harmonic/sequence components under highly polluted and unbalanced grid will be obtained and its structure is depicted in Fig. 7.

As can be inferred from Fig. 7, the main configuration of the three-phase MGDSS-PLL is similar to the single-phase MGDSS-PLL introduced previously. Hence, the signal processing procedure of the three-phase MGDSS-PLL can be equally concluded and described as follows.

1) Three-phase input signal V_{abc} is transferred to $V_{\alpha\beta}$ under the $\alpha\beta$ reference frame using the *Clark* transformation and then fed to the multiple GDSS-PNSC subsystems.
2) Irrelevant harmonic components contained in $V_{\alpha\beta}$ will be eliminated by the GDSS operators in each GDSS-PNSC subsystem and pure quadrature signals at targeted frequencies will be generated. Then, these quadrature signals will be extracted into positive and negative sequence components under the $\alpha\beta$ reference frame by the PNSC blocks as shown in (13) and (14).
3) The same type of SRF-PLL structure as mentioned in single-phase MGDSS-PLL is implemented here to track the positive fundamental phase θ^+. Since the input signal $V^+_{\alpha\beta}$ is clean and balanced, a similar design procedure is applied as in single-phase applications.

TABLE II
SINGLE-PHASE GRID PARAMETERS

Voltage components	Magnitudes (V)	Phase (rad)
Fundamental voltage	311	0
Third harmonic	62	$\pi/6$
Fifth harmonic	62	$\pi/4$
Seventh harmonic	62	0
Ninth harmonic	31	$\pi/6$
Eleventh harmonic	31	$\pi/12$
Thirteenth harmonic	31	$\pi/9$
Fifteenth harmonic	62	$\pi/3$

4) The obtained positive and negative harmonic sequence components at multiple desired orders are finally transferred to the *abc* stationary reference frame.

As can be seen from Figs. 5 and 7, the fundamental synchronization is realized through a typical SRF-PLL structure, and its accuracy is actually ensured by the GDSS operator tuned at the fundamental frequency, while other GDSS operators designed at multiple harmonic frequencies are only implemented for estimating multiple harmonic components in order to be used in the control process. Therefore, the performance of the MGDSS-PLL is basically determined by the GDSS operators, and thus the MGDSS-PLL can be flexibly designed with a variable number of GDSS-PNSC or GDSS subsystems for the specific applications and the control requirements. Furthermore, the parameters of the GDSS operators can also be optimized according to the different grid conditions and the control requirements, in order to achieve the most suitable synchronization performance in respect to the tracking accuracy and computational complexity. It is worth mentioning that the MGDSS-PLL is immune to the input frequency variations within a small range, since the gains and phases around the targeted frequencies are still close to their nominal values as shown in Figs. 3 and 4.

Consequently, with the adoption of the proposed GDSS operators, fast dynamic and accurate synchronization for both fundamental and multiple harmonic components can be guaranteed simultaneously, even under highly harmonic distortion or typical grid disturbances.

IV. SIMULATION AND EXPERIMENTAL VERIFICATION

To verify the performance of the MGDSS-PLL under adverse grid conditions, simulations based on MATLAB/SIMULINK and experimental tests with a *dSPACE* DS 1103 system are presented in this section. In the simulations and experiments, a highly unbalanced and distorted grid is applied, and the grid parameters during normal and fault conditions are specified in Table II for single-phase systems and in Table III for three-phase systems. The MGDSS-PLL is configured to track the fundamental, third, fifth, seventh, and ninth harmonic components in single-phase systems and to track the fundamental, fourth, seventh, and eleventh harmonic sequence components in three-phase systems. Moreover, parameters of the GDSS operators in the single-phase applications are listed in Table IV, and parameters of GDSS-PNSC subsystems in the three-phase applications

TABLE III
THREE-PHASE GRID PARAMETERS

Voltage components	Magnitudes (V)	Phase (rad)
Fundamental positive sequence	311	0
Fundamental negative sequence	40	$\pi/3$
Second harmonic positive sequence	31	0
Fourth harmonic negative sequence	31	$\pi/6$
Fifth harmonic positive sequence	62	$\pi/6$
Seventh harmonic negative sequence	62	$\pi/4$
Eighth harmonic positive sequence	31	$\pi/3$
Eleventh harmonic positive sequence	62	$\pi/12$
Thirteenth harmonic negative sequence	62	$\pi/9$

TABLE IV
PARAMETERS OF THE SINGLE-PHASE MGDSS-PLL

GDSS submodular	m	n	h_i (even orders excluded)
GDSS-QSG	12	26	1, 25, 27 ...
$GDSS1_3$	14	10	3, 27, 33 ...
$GDSS1_5$	14	6	5, 25, 35 ...
$GDSS1_7$	20	6	7, 35, 49 ...
$GDSS1_9$	17	4	9, 27, 45 ...

TABLE V
COMPLEXITY OF THE SINGLE-PHASE AND THREE-PHASE MGDSS-PLL

Application	[GDSS]	[PNSC]	$[T_{\alpha\beta}$ & $T_{\alpha\beta}^{-1}]$	Total multiplications	Total additions
Single phase	6	0	0	22	80
Three phase	16	4	6	69	282

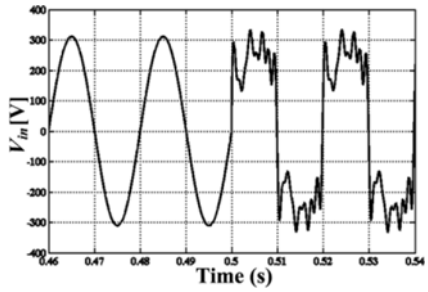

Fig. 8. Highly distorted single-phase grid voltage.

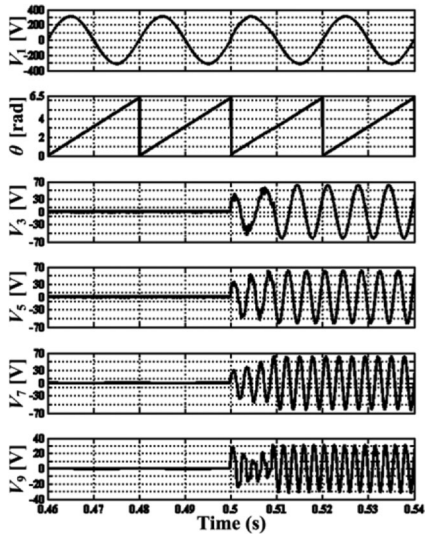

Fig. 9. Simulation results of the single-phase MGDSS-PLL under distorted grid conditions.

are provided in Table I. The grid fundamental frequency is 50 Hz during the simulations and experiments.

Before the simulation and experimental results are demonstrated, computational complexity of the MGDSS-PLL should be analyzed to evaluate its real-time process, since hardware resources are generally limited in practical applications. According to Fig. 5, the process of single-phase MGDSS-PLL mainly requires to compute one GDSS-QSG submodular and four *GDSS1* operators. Meanwhile, based on Fig. 7, the process of three-phase MGDSS-PLL practically requires calculating six transformation matrices and four GDSS-PNSC subsystems. As can be inferred from (12), the proposed GDSS operator consists of two parts: Sampling points stored in the memory and constant coefficients that can be determined during the design process. Therefore, the process of the GDSS operator can simply be realized with $(m + 1)$ multiplications and m additions. Actually, the mathematical operations of the GDSS operator can be further decreased considering the symmetrical characteristics of the coefficients.

Consequently, the complexity of the single-phase and three-phase MGDSS-PLL can be summarized and as presented in Table V. As can be seen from the results, the processing time of the synchronization algorithm is relevantly short according to the complexity analysis discussed in [37], which is beneficial for the real-time operation of the control system.

A. Simulation Results

Single-phase distorted grid voltage described in Table II is illustrated in Fig. 8, where the grid fault appears at $t = 0.5$ s. Simulation results of the MGDSS-PLL under this grid condition are shown in Fig. 9. As can be seen from the results, MGDSS-PLL can accurately synchronize with the fundamental phase and extract multiple targeted harmonics within half a fundamental cycle, which is consistent with the theoretical analysis. In order to further test the performance of MGDSS-PLL under adverse grid conditions, grid disturbances including voltage sag, phase jump, and frequency variation are applied in the simulation and the results are given in Figs. 10 and 11. In Fig. 10, at $t = 0.5$ s, the grid fundamental voltage peak value drops from 311 to 255 V with an extra $\pi/6$ phase jump and in Fig. 11, the grid fundamental frequency changes from 50 to 50.5 Hz during the fault condition. As can be seen from Figs. 10 and 11, the proposed MGDSS-PLL is valid in single-phase distorted grid and exhibits great robustness considering common grid disturbances.

Similar simulation tests are set up for three-phase applications. The unbalanced and distorted grid specified in Table III is shown in Fig. 12, where the grid fault appears at $t = 0.5$ s. Simulation results of the MGDSS-PLL under this extreme grid condition are given in Fig. 13. As indicated by the simulation waveforms, the proposed MGDSS-PLL can accurately extract

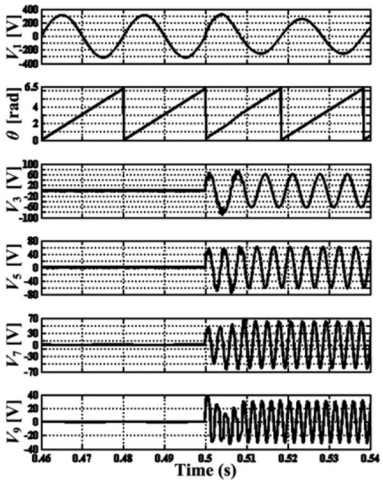

Fig. 10. Simulation results of the single-phase MGDSS-PLL with voltage sag and phase jump.

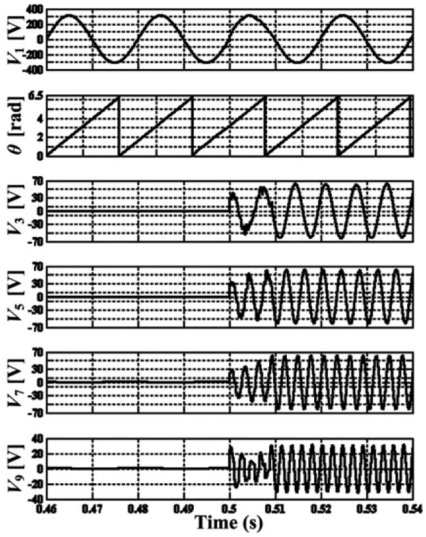

Fig. 11. Simulation results of the single-phase MGDSS-PLL with frequency change.

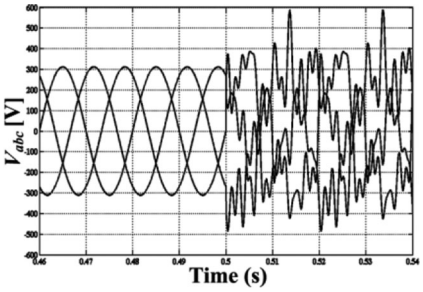

Fig. 12. Unbalanced and distorted three-phase grid voltage.

all the interested harmonic sequence components within one fundamental period, which is also consistent with the theoretical analysis. Then, the MGDSS-PLL is tested under more stringent scenarios with grid voltage sag, phase jump, and frequency variation. The obtained results are demonstrated in Figs. 14 and 15. In Fig. 14, the grid positive fundamental voltage drops from

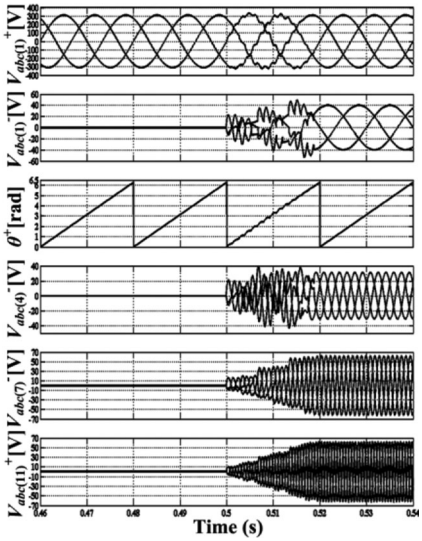

Fig. 13. Simulation of the three-phase MGDSS-PLL under abnormal grid condition.

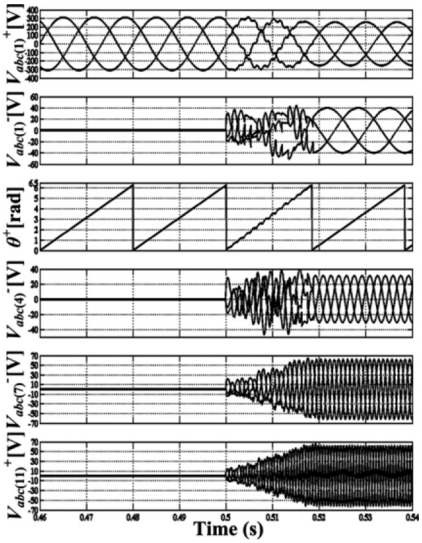

Fig. 14. Simulation of the three-phase MGDSS-PLL with voltage sag and phase jump.

311 to 255 V with an extra $\pi/6$ phase jump at $t = 0.5$ s. The other conditions remain the same as given in Table III. The same parameters are set for the grid voltage in Fig. 15 except that the positive fundamental frequency changes from 50 to 50.5 Hz during the fault condition. As can be concluded from Figs. 14 and 15, the introduced MGDSS-PLL can effectively work in three-phase grid under a variety of grid conditions, which makes it an attractive synchronization technique.

B. Experimental Results

During the experiments, the input voltage is sampled by the analog-to-digital converters and fed to the detection algorithm. The waveforms recorded are all calculated results based on the detection algorithm and generated by the digital-to-analog

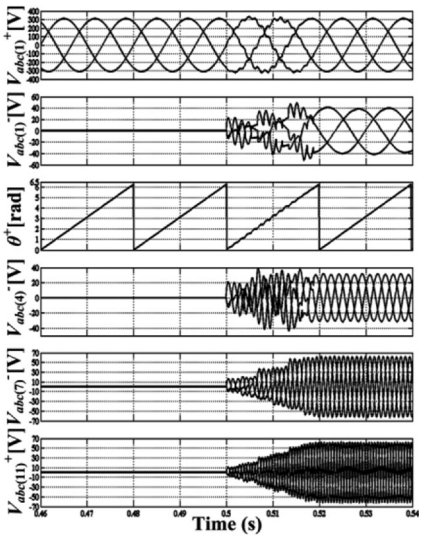

Fig. 15. Simulation of the three-phase MGDSS-PLL with frequency change.

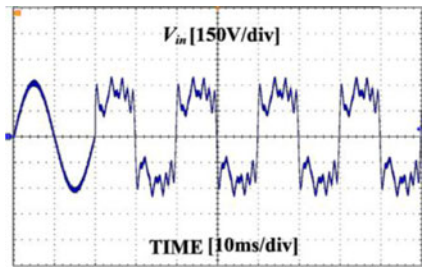

Fig. 16. Distorted single-phase grid voltage in the experiments.

converters of the control system. The sampling rate in the experiments is set to 15 kHz.

Single-phase distorted input voltage applied in the experiments is given in Fig. 16, and its parameters are described in Table II. Experimental results of the single-phase MGDSS-PLL under this condition are provided in Fig. 17. According to the results, the proposed MGDSS-PLL can effectively detect the fundamental phase and extract multiple interested harmonic components within half a fundamental period, which is also proved by the simulation results. Fig. 18 shows the experimental results of the single-phase MGDSS-PLL under a more exigent situation, where the grid fundamental voltage drops from 311 to 255 V with an extra $\pi/6$ phase delay and 0.5 Hz frequency change. As indicated by the waveforms, the detection performance is not affected and the MGDSS-PLL algorithm shows great robustness.

The unbalanced and distorted three-phase input voltages used in the experiment is demonstrated in Fig. 19, and its important parameters are given in Table III. Fig. 20 shows the experimental results of the proposed method under the input voltage given in Fig. 19. As can be seen from the waveforms, all the positive- and negative sequence components contained in the input are accurately separated by the MGDSS-PLL and the settling time of the algorithm is about one fundamental period, which matches with the simulation and theoretical analysis. A more critical grid condition is also tested in the experiments and the results are

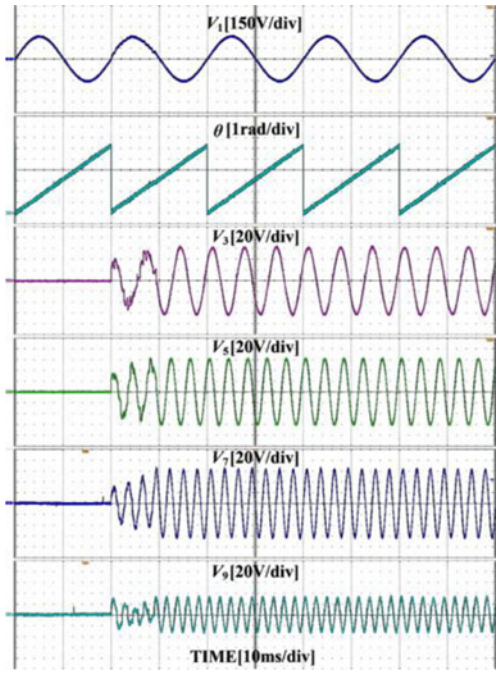

Fig. 17. Experimental results of the single-phase MGDSS-PLL under distorted grid conditions.

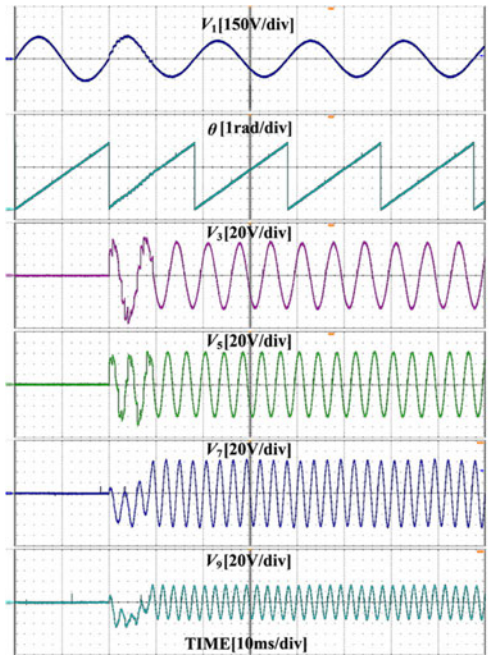

Fig. 18. Experimental results of the single-phase MGDSS-PLL with extra perturbations.

demonstrated in Fig. 21, where the grid positive fundamental voltage drops from 311 to 255 V with an extra $\pi/6$ phase jump and 0.5 Hz frequency change. As it can be confirmed by Fig. 21, the introduced MGDSS-PLL is immune to some typical grid perturbations like voltage sag, phase jump and small frequency variation, so it can maintain high tracking performance with great robustness.

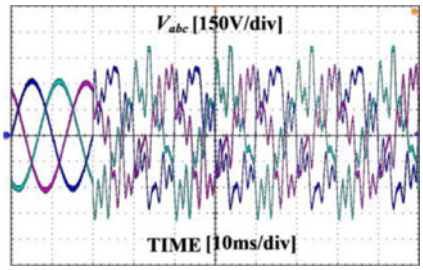

Fig. 19. Unbalanced and distorted three-phase grid voltage in the experiments.

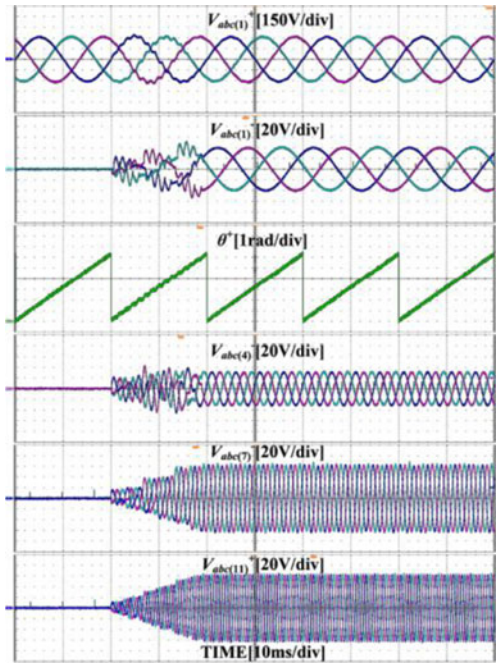

Fig. 20. Experimental results of three-phase MGDSS-PLL with an abnormal grid.

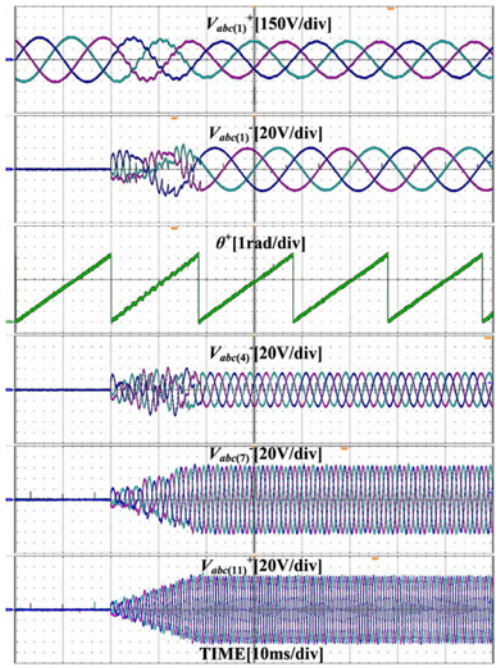

Fig. 21. Experimental results of three-phase MGDSS-PLL with grid perturbations.

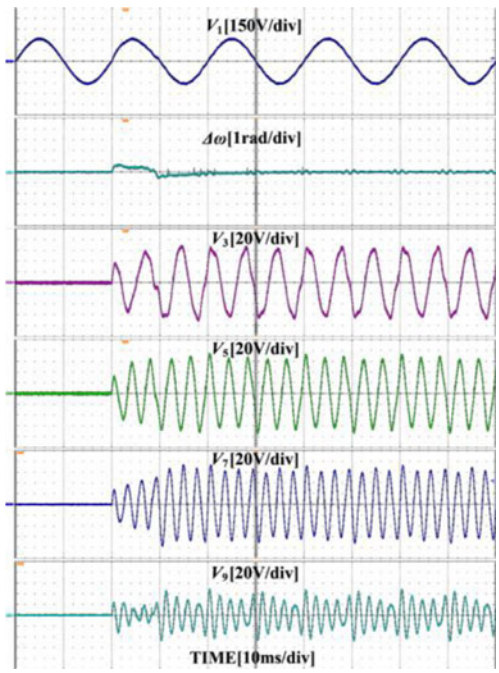

Fig. 22. Experimental results of the MSOGI-FLL with a single-phase grid.

As illustrated by the simulation and experimental results given in Figs. 8–21, the proposed MGDSS-PLL can maintain excellent synchronization performance under extremely distorted single-phase/three-phase applications and exhibits great robustness against different grid perturbations. Furthermore, the response time is half the fundamental period for single-phase MGDSS-PLL and one fundamental cycle for three-phase MGDSS-PLL, which indicates a faster dynamic than the methods proposed in [35]–[37] as mentioned in Section I.

To make it more clearly about the benefits of the derived MGDSS-PLL structure, the input voltages shown in Figs. 16 and 19 are also tested with the aforementioned MSOGI-FLL. The obtained experimental results are, respectively, presented in Figs. 22 and 23, where $\Delta\omega^{+} = (\omega - 314.16)\,\mathrm{rad/s}$ represents the error between detected positive fundamental frequency and its rated value. In the experiments, only the fundamental, third, fifth, seventh, and ninth harmonics are considered to design the HDN of the single-phase MSOGI-FLL, and only the fundamental, fourth, seventh, and eleventh harmonics are considered to design the HDN of the three-phase MSOGI-FLL. All other harmonic components contained are regarded as unknown components. According to the obtained results, any unconsidered harmonics will affect the tracking performance of the MSOGI-FLL when the number of DSOGI subsystems is not equal to the number of significant harmonic components contained.

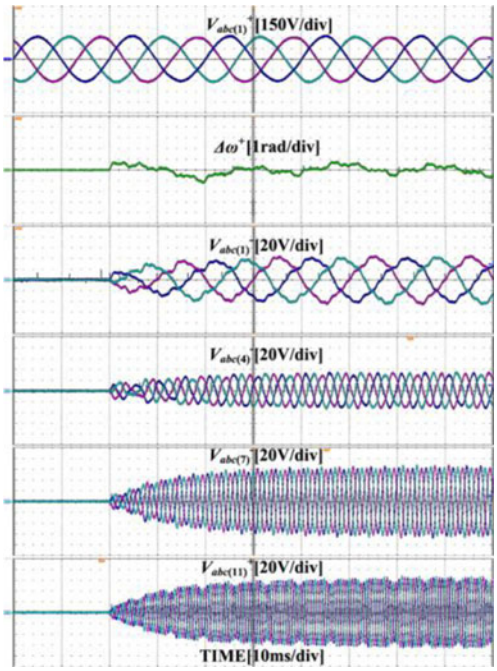

Fig. 23. Experimental results of the MSOGI-FLL with a three-phase grid.

V. Conclusion

This paper has presented two types of GDSS operators that can extract any arbitrary harmonic component out of the input signal and they can flexibly be configured to improve the performance of synchronization and harmonic detection algorithms with fast dynamic (response time as short as half a fundamental cycle). A new grid information estimation system based on the introduced GDSS operators, i.e., MGDSS-PLL, has also been proposed for the fundamental and multiple harmonics detection under extremely polluted single-phase and three-phase grid conditions.

The proposed MGDSS-PLL structure contains multiple GDSS operators working collaboratively, which enables accurate and fast signal extraction at multiple interested harmonic orders. Since these GDSS operators are quite selective, the design process of each GDSS block is independent, and there will be no interaction between different harmonic components. Hence, the obtained MGDSS-PLL is insensitive to unconsidered harmonic components. Moreover, the MGDSS-PLL also exhibits great robustness regarding to typical abnormal grid conditions including voltage sags, phase jumps, and frequency variations. All these features make the proposed MGDSS-PLL to be a competitive synchronization algorithm for both single-phase and three-phase systems in practical applications. Simulation and experimental results under varieties of grid conditions are presented in the paper to verify the effectiveness of the GDSS operators and the proposed MGDSS-PLL.

References

[1] F. Blaabjerg, Z. Chen, and S. B. Kjaer, "Power electronics as efficient interface in dispersed power generation systems," *IEEE Trans. Power Electron.*, vol. 19, no. 5, pp. 1184–1194, Sep. 2004.

[2] J. Carrasco *et al.*, "Power-electronic systems for the grid integration of renewable energy sources: A survey," *IEEE Trans. Ind. Electron.*, vol. 53, no. 4, pp. 1002–1016, Jun. 2006.

[3] A. Timbus, M. Liserre, R. Teodorescu, P. Rodriguez, and F. Blaabjerg, "Evaluation of current controllers for distributed power generation systems," *IEEE Trans. Power Electron.*, vol. 24, no. 3, pp. 654–664, Mar. 2009.

[4] P. Acuna, L. Moran, M. Rivera, J. Dixon, and J. Rodriguez, "Improved active power filter performance for renewable power generation systems," *IEEE Trans. Power Electron.*, vol. 29, no. 2, pp. 687–694, Feb. 2014.

[5] *IEEE Standard for Interconnecting Distributed Resources With Electric Power Systems*, IEEE Std. 1547-2003, 2003.

[6] M. Tsili and S. Papathanassiou, "A review of grid code technical requirements for wind farms," *IET Renew. Power Gener.*, vol. 3, no. 3, pp. 308–332, Sep. 2009.

[7] B.-I. Craciun, T. Kerekes, D. Sera, and R. Teodorescu, "Overview of recent grid codes for PV power integration," in *Proc. 13th Int. Conf. Optim. Elect. Electron. Equip.*, Brasov, Romania, 2012, pp. 959–965.

[8] K.-H. Kim, Y.-C. Jeung, D.-C. Lee, and H.-G. Kim, "LVRT scheme of PMSG wind power systems based on feedback linearization," *IEEE Trans. Power Electron.*, vol. 27, no. 5, pp. 2376–2384, May 2012.

[9] D. Santos-Martin, J. L. Rodriguez-Amenedo, and S. Arnaltes, "Direct power control applied to doubly fed induction generator under unbalanced grid voltage conditions," *IEEE Trans. Power Electron.*, vol. 23, no. 5, pp. 2328–2336, Sep. 2008.

[10] P. Rodriguez, A. Timbus, R. Teodorescu, M. Liserre, and F. Blaabjerg, "Flexible active power control of distributed power generation systems during grid faults," *IEEE Trans. Ind. Electron.*, vol. 54, no. 5, pp. 2583–2592, Oct. 2007.

[11] L. Asiminoaei, F. Blaabjerg, and S. Hansen, "Detection is key—Harmonic detection methods for active power filter applications," *IEEE Ind. Appl. Mag.*, vol. 13, no. 4, pp. 22–33, Jul./Aug. 2007.

[12] F. Blaabjerg, R. Teodorescu, M. Liserre, and A. Timbus, "Overview of control and grid synchronization for distributed power generation systems," *IEEE Trans. Ind. Electron.*, vol. 53, no. 5, pp. 1398–1409, Oct. 2006.

[13] X. Q. Guo, W. Y. Wu, X. F. Sun, and G. C. San, "Phase locked loop for electronically-interfaced converters in distributed utility network," in *Proc. Int. Conf. Elect. Mach. Syst.*, Oct. 2008, pp. 2346–2350.

[14] S. Alepuz *et al.*, "Control strategies based on symmetrical components for grid-connected converters under voltage dips," *IEEE Trans. Ind. Electron.*, vol. 56, no. 6, pp. 2162–2173, Jun. 2009.

[15] K.-J. Lee, J.-P. Lee, D. Shin, D.-W. Yoo, and H.-J. Kim, "A novel grid synchronization PLL method based on adaptive low-pass notch filter for grid connected PCS," *IEEE Trans. Ind. Electron.*, vol. 61, no. 1, pp. 292–301, Jan. 2014.

[16] R. M. S. Filho, P. F. Seixas, P. C. Cortizo, L. A. B. Torres, and A. F. Souza, "Comparison of three single-phase PLL algorithms for UPS applications," *IEEE Trans. Ind. Electron.*, vol. 55, no. 8, pp. 2923–2932, Aug. 2008.

[17] S. Chung, "A phase tracking system for three phase utility interface inverters," *IEEE Trans. Power Electron.*, vol. 15, no. 3, pp. 431–438, May 2000.

[18] V. Kaura and V. Blasko, "Operation of a phase locked loop system under distorted utility conditions," *IEEE Trans. Ind. Appl.*, vol. 33, no. 1, pp. 58–63, Jan./Feb. 1997.

[19] M. A. Perez, J. R. Espinoza, L. A. Moran, M. A. Torres, and E. A. Araya, "A robust phase-locked loop algorithm to synchronize static-power converters with polluted AC systems," *IEEE Trans. Power Electron.*, vol. 55, no. 5, pp. 2185–2192, May 2008.

[20] P. Rodriguez, J. Pou, J. Bergas, J. Candela, R. Burgos, and D. Boroyevich, "Decoupled double synchronous reference frame PLL for power converters control," *IEEE Trans. Power Electron.*, vol. 22, no. 2, pp. 584–592, Mar. 2007.

[21] X. Guo, W. Wu, and Z. Chen, "Multiple-complex coefficient-filter-based phase-locked loop and synchronization technique for three-phase grid interfaced converters in distributed utility networks," *IEEE Trans. Ind. Electron.*, vol. 58, no. 4, pp. 1194–1204, Apr. 2011.

[22] A. V. Timbus, M. Liserre, R. Teodorescu, and F. Blaabjerg, "Synchronization methods for three phase distributed power generation systems. An overview and evaluation," in *Proc. IEEE Power Electron. Spec. Conf.*, 2005, pp. 2474–2481.

[23] M. Karimi-Ghartemani, H. Karimi, and A. Bakhshai, "A filtering technique for three-phase power systems," *IEEE Trans. Instrum. Meas.*, vol. 58, no. 2, pp. 389–396, Feb. 2009.

[24] S. Golestan, M. Ramezani, J. M. Guerrero, and M. Monfared, "DQ-frame cascaded delayed signal cancellation-based PLL: Analysis, design, and comparison with moving average filter-based PLL," *IEEE Trans. Power Electron.*, vol. 30, no. 3, pp. 1618–1632, Mar. 2015.
[25] W. Li, X. Ruan, C. Bao, D. Pan, and X. Wang, "Grid synchronization systems of three-phase grid-connected power converters: A complex vectorfilter perspective," *IEEE Trans. Ind. Electron.*, vol. 61, no. 4, pp. 1855–1870, Apr. 2014.
[26] P. Rodriguez, J. Pou, J. Bergas, I. Candela, R. Burgos, and D. Boroyevic, "Double synchronous reference frame PLL for power converters control," in *Proc. IEEE Power Electron. Spec. Conf.*, 2005, pp. 1415–1421.
[27] R. Bojoi, L. Limongi, D. Roiu, and A. Tenconi, "Enhanced power quality control strategy for single-phase inverters in distributed generation systems," *IEEE Trans. Power Electron.*, vol. 26, no. 3, pp. 798–806, Mar. 2011.
[28] B. Liu, F. Zhuo, Y. Zhu, H. Yi, and F. Wang, "A Three-phase PLL algorithm based on signal reforming under distorted grid conditions," *IEEE Trans. Power Electron.*, vol. 30, no. 9, pp. 5272–5283, Sep. 2015.
[29] S. Golestan, M. Ramezani, J. M. Guerrero, F. D. Freijedo, and M. Monfared, "Moving average filter based phase-locked loops: Performance analysis and design guidelines," *IEEE Trans. Power Electron.*, vol. 29, no. 6, pp. 2750–2763, Sep. 2014.
[30] S. Golestan, J. M. Guerrero, A. Vidal, A. G. Yepes, and J. Doval-Gandoy, "PLL with MAF-based prefiltering stage: Small-signal modeling and performance enhancement," *IEEE Trans. Power Electron.*, vol. 31, no. 6, pp. 4013–4019, Sep. 2016.
[31] P. Rodriguez, A. Luna, M. Ciobotaru, R. Teodorescu, and F. Blaabjerg, "Advanced grid synchronization system for power converters under unbalanced and distorted operating conditions," in *Proc. 32nd Annu. Conf. IEEE Ind. Electron.*, Nov. 2006, pp. 5173–5178.
[32] P. Rodriguez, R. Teodorescu, I. Candela, A. V. Timbus, M. Liserre, and F. Blaabjerg, "New positive-sequence voltage detector for grid synchronization of power converters under faulty grid conditions," in *Proc. IEEE Power Electron. Spec. Conf.*, 2006, pp. 1–7.
[33] Y. F. Wang and Y. W. Li, "Grid synchronization PLL based on cascaded delayed signal cancellation," *IEEE Trans. Power Electron.*, vol. 26, no. 7, pp. 1987–1997, Jul. 2011.
[34] F. A. S. Neves, M. C. Cavalcanti, H. E. P. de Souza, F. Bradaschia, E. J. Bueno, and M. Rizo, "A generalized delayed signal cancellation method for detecting fundamental-frequency positive-sequence three-phase signals," *IEEE Trans. Power Del.*, vol. 25, no. 3, pp. 1816–1825, Jul. 2010.
[35] P. Rodriguez, A. Luna, I. Candela, R. Mujal, R. Teodorescu, and F. Blaabjerg, "Multiresonant frequency-locked loop for grid synchronization of power converters under distorted grid conditions," *IEEE Trans. Ind. Electron.*, vol. 58, no. 1, pp. 127–138, Jan. 2011.
[36] L. Hadjidemetriou, E. Kyriakides, and F. Blaabjerg, "A robust synchronization to enhance the power quality of renewable energy systems," *IEEE Trans. Ind. Electron.*, vol. 62, no. 8, pp. 4858–4868, Apr. 2015.
[37] L. Hadjidemetriou, Y. H. Yang, E. Kyriakides, and F. Blaabjerg, "A synchronization scheme for single-phase grid-tied inverters under harmonic distortion and grid disturbances," *IEEE Trans. Power Electron.*, vol. 32, no. 4, pp. 2784–2793, Jan. 2017.
[38] Y. Lu, G. C. Xiao, L. F. Zang, X. L. Wu, and F. W. Chen, "A novel synchronization method designed for single-phase distorted grid," in *Proc. IEEE Appl. Power Electron. Conf. Expo.*, 2015, pp. 2866–2871.
[39] Y. Wang and Y. Li, "Three-phase cascaded delayed signal cancellation PLL for fast selective harmonic detection," *IEEE Trans. Ind. Electron.*, vol. 60, no. 4, pp. 1452–1463, Apr. 2013.
[40] I. S. Gradshteyn and I. M. Ryzhik, *Table of Integrals, Series, and Products*. San Diego, CA, USA: Academy Press, 2007.
[41] P. Zahradnik and M. Vlcek, "Analytical design of optimal FIR combfilters," in *Proc. IEEE Int. Conf. Commun.* , 2003, vol. 5, pp. 3590–3593

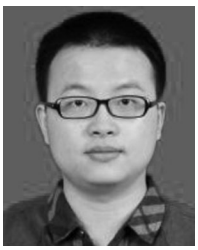

Yong Lu received the B.S., M.S., and Ph.D. degrees from the School of Electrical Engineering, Xi'an Jiaotong University, Xi'an, China, in 2010, 2012, and 2016, respectively, all in electrical engineering.

He is currently a Faculty Member of School of Electronics and Control Engineering, Chang'an University, Xi'an.

His research interests include power quality, control of the power converters, and distributed generation.

Guochun Xiao (M'06) was born in Sichuan Province, China, in 1965. He received the B.S., M.S., and Ph.D. degrees from the School of Electrical Engineering, Xi'an Jiaotong University, Xi'an, China, in 1987, 1990, and 2002, respectively.

From 1990 to 1998, he was an Engineer at the Xi'an Electric Furnace Research Institute. He is currently a full Professor at Xi'an Jiaotong University. His current research interests include power conversion systems, harmonics suppression, reactive power compensation, and active power filters.

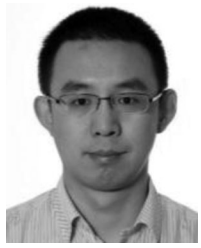

Xiongfei Wang (S'10–M'13–SM'17) received the B.S. degree from Yanshan University, Qinhuangdao, China, in 2006, the M.S. degree from Harbin Institute of Technology, Harbin, China, in 2008, both in electrical engineering, and the Ph.D. degree in energy technology from Aalborg University, Aalborg, Denmark, in 2013.

Since 2009, he has been with the Aalborg University, where he is currently an Associate Professor in the Department of Energy Technology. His research interests include modeling and control of grid-connected converters, harmonics analysis and control, passive and active filters, and stability of power electronic-based power systems.

Dr. Wang serves as an Associate Editor for the IEEE TRANSACTIONS ON POWER ELECTRONICS, the IEEE TRANSACTIONS ON INDUSTRY APPLICATIONS, and the IEEE JOURNAL OF EMERGING AND SELECTED TOPICS IN POWER ELECTRONICS. He is also the Guest Editor for the Special Issue "Grid-Connected Power Electronics Systems: Stability, Power Quality, and Protection" in the IEEE TRANSACTIONS ON INDUSTRY APPLICATIONS. He received the second prize paper award and the outstanding reviewer award of IEEE Transactions on Power Electronics in 2014 and 2017, respectively, and the best paper awards at IEEE Power Electronics for Distributed Generation Systems 2016 and IEEE Power and Energy Society General Meeting 2017.

Frede Blaabjerg (S'86–M'88–SM'97–F'03) received Ph.D. degree in electrical engineering from Aalborg University, Aalborg, Denmark, in 1992.

From 1987 to 1988, he was with ABB-Scandia, Randers, Denmark. He became an Assistant Professor, in 1992, an Associate Professor, in 1996, and a Full Professor of power electronics and drives, in 1998.In 2017, he became a Villum Investigator. His current research interests include power electronics and its applications such as in wind turbines, photovoltaic systems, reliability, harmonics, and adjustable speed drives. He has published more than 450 journal papers in the fields of power electronics and its applications. He is the coauthor of two monographs and editor of six books in power electronics and its applications.

Dr. Blaabjerg received 18 IEEE Prize Paper Awards, the IEEE PELS Distinguished Service Award in 2009, the EPE-PEMC Council Award in 2010, the IEEE William E. Newell Power Electronics Award 2014, and the Villum Kann Rasmussen Research Award 2014. He was the Editor-in-Chief of the IEEE TRANSACTIONS ON POWER ELECTRONICS, from 2006 to 2012. He has been a Distinguished Lecturer for the IEEE Power Electronics Society from 2005 to 2007 and for the IEEE Industry Applications Society, from 2010 to 2011 as well as 2017 to 2018. He was nominated in 2014, 2015, and 2016 by Thomson Reuters to be between the most 250 cited researchers in Engineering in the world. In 2017, he became Honoris Causa at University Politehnica Timisoara, Romania.